Terahertz substance imaging by waveform shaping

Minwoo Yi,[1] Hyosub Kim,[1] Kyong Hwan Jin,[2] Jong Chul Ye,[2] and Jaewook Ahn[1,*]

[1]*Department of Physics, KAIST, Daejeon 305-701 Korea*
[2]*Department of Bio and Brain Engineering, KAIST, Daejeon 305-701, Korea*
[*]*jwahn@kaist.ac.kr*

Abstract: Terahertz pulse shaping technique is used to adaptively design terahertz waveforms of enhanced spectral correlation to particular materials among a given set of materials. In a proof-of-principle experiment performed with a two-dimensional image target consisted of meta-materials of distinctive resonance frequencies, the as-designed waveforms are used to demonstrate terahertz substance imaging. It is hoped that this material-specific terahertz waveforms may enable single- or few-shot terahertz material classification when being used in conjunction with terahertz power measurement.

OCIS codes: (110.6795) Terahertz imaging; (160.3918) Metamaterials; (320.0320) Ultrafast optics; (320.5540) Pulse shaping.

References and links

1. Y.-S. Lee, *Principles of Terahertz Science and Technology* (Springer, USA, 2009).
2. D. Grischkowsky, S. Keiding, M. van Exter, and Ch. Fattinger, "Far-infrared time-domain spectroscopy with terahertz beams of dielectrics and semiconductors," J. Opt. Soc. Am. B **7**, 2006 (1990).
3. B. Ferguson and X.-C. Zhang, "Materials for terahertz science and technology," Nat. Mater. **1**, 26-33 (2002).
4. M. Tonouchi, "Cutting-edge terahertz technology," Nat. Photon. **1**, 97105 (2007).
5. K. Kawase, Y. Ogawa, Y. Watanabe, and H. Inoue, "Non-destructive terahertz imaging of illicit drugs using spectral fingerprints," Opt. Express **11**, 2549–2554 (2003).
6. A. M. Weiner, J. P. Heritage, and J. A. Salehi, "Encoding and decoding of femtosecond pulses," Opt. Lett. **13**, 300–302 (1988).
7. R. Bartels, S. Backus, E. Zeek, L. Misoguti, G. Vdovin, I. P. Christov, M. M. Murnane, and H. C. Kapteyn, "Shaped pulse optimization of coherent emission of high-harmonic soft X-rays," Nature **406**, 164-166 (2000).
8. D. Meshulach and Y. Silberberg, "Coherent quantum control of two-photon transitions by a femtosecond laser pulse," Nature **396**, 239–242 (1998).
9. S. Lee, J. Lim, J. Ahn, V. Hakobyan, and S. Guerin, "Strong-field two-level two-photon transition by phase shaping," Phys. Rev. A **82**, 023408 (2010).
10. J. Lim, H.-g. Lee, S. Lee, and J. Ahn, "Quantum control in two-dimensional Fourier transform spectroscopy," Phys. Rev. A **84**, 013425 (2011).
11. J. P. Ogilvie, D. Débarre, X. Solinas, J.-L. Martin, E. Beaurepaire, and M. Joffre, "Use of coherent control for selective two-photon fluorescence microscopy in live organisms," Opt. Express **14**, 759–766 (2006).
12. J. Ahn, A. Efimov, R. Averitt, and A. Taylor, "Terahertz waveform synthesis via optical rectification of shaped ultrafast laser pulses," Opt. Express **11**, 2486-2496 (2003).
13. K. K. Kohli, A. Vaupel, S. Chatterjee, and W. W. Rühle, "Adaptive shaping of THz-pulses generated in <110> ZnTe crystals," J. Opt. Soc. Am. B **26**, A74–A78 (2009).
14. S. Vidal, J. Degert, J. Oberlè, and E. Freysz, "Femtosecond optical pulse shaping for tunable terahertz pulse generation," J. Opt. Soc. Am. B **27**, 1044–1050 (2010).
15. M. Yi, K. Hee Lee, I. Maeng, J.-H. Son, R. D. Averitt, and J. Ahn, "Tailoring the spectra of terahertz emission from CdTe and ZnTe electro-optic crystals," Jpn. J. Appl. Phys. **47**, 202–204 (2008).

#167967 - $15.00 USD Received 4 May 2012; revised 31 Jul 2012; accepted 20 Aug 2012; published 24 Aug 2012

16. Y. Liu, S.-G. Park, and A. M. Weiner, "Terahertz waveform synthesis via optical pulse shaping," IEEE J. Sel. Top. Quantum Electron. **2**, 709–719 (1996).
17. J. Y. Sohn, Y. H. Ahn, D. J. Park, E. Oh, and D. S. Kim, "Tunable terahertz generation using femtosecond pulse shaping," Appl. Phys. Lett. **81**, 13–15 (2002).
18. C. D'Amico, M. Tondusson, J. Degert, and E. Freysz, "Tuning and focusing THz pulses by shaping the pump laser beam profile in a nonlinear crystal," Opt. Express **17**, 592–597 (2009).
19. Y.-S. Lee, N. Amer, and W. C. Hurlbut, "Terahertz pulse shaping via optical rectification in poled lithium niobate," Appl. Phys. Lett. **82**, 170–172 (2003).
20. M. Yamaguchi and J. Das, "Terahertz wave generation in nitrogen gas using shaped optical pulses," J. Opt. Soc. Am. B **26**, A90–A94 (2009).
21. W. J. Padilla, M. T. Aronsson, C. Highstrete, M. Lee, A. J. Taylor, and R. D. Averitt, "Electrically resonant terahertz metamaterials: Theoretical and experimental investigations," Phys. Rev. B **75**, 041102(R) (2007).
22. A. M. Weiner, "Femtosecond pulse shaping using spatial light modulators," Rev. Sci. Instrum. **71**, 1929–1960 (2000).
23. E. Hecht, *Optics* 4th ed. (Addison Wesley, 2002).
24. M. Mitchell, *An Introduction to Genetic Algorithms* (MIT Press, 1996).

1. Introduction

Recent advances in science and technology of terahertz (THz) frequency wave have made impactful contributions to a variety of research areas including physics, chemistry, material science, and electric engineering [1]. Because of the spectral richness of many materials in THz frequency range, THz time-domain spectroscopy (THz-TDS) has become one of the essential analyzing tools in material science nowadays [2], and its applications are particularly promising in biological and medical imaging, nondestructive inspection, and hazardous material classification to list [3–5]. Although THz-TDS is a powerful technique of high-resolution spectroscopy, its temporal profile measurement of electric fields is often time-consuming. However, some THz-TDS applications, for example, material identification may not require a full measurement of the THz spectral response function of an unknown material, but instead comparing its spectral correlations to an archived THz spectral database of a classified materials may be enough. In that regards, transmissive THz power detection with a series of pre-determined THz waveforms coupled to the material database can simply identify the unknown material. Therefore, one could consider adaptive pulse-shaping technique to design a set of THz waveforms of material-specific spectral correlations and use those shaped THz pulses for substance imaging, which is the subject of the present paper.

As for the pulse-shaping, there has been much interest in optical frequency domain, in part because of its applications in telecommunication and signal processing [6], and in part because of its potential use as a new optical means toward selective control of electronic and vibrational response of materials [7–10]. Of particular relevance in the context of the present paper is the coherent control spectroscopy introduced by Ogilvie and co-workers, where the nonlinear nature of two-photon fluorescence provided by shaped optical fields has been exploited for selective substance microscopy of biological materials [11]. In THz frequency region, several methods have been developed for the generation of arbitrary THz waveforms, most of which are based on THz emission by spatially and/or temporally shaped optical pulses [12–18], or tunable THz waveform generation from quasi-phase matching process [19], or air-plasma breakdown phenomena [20]. However, there are few practical imaging methodologies which explicitly take the full advantage of pulse-shaping capability.

In this paper, we consider THz waveform shaping for the purpose of material classification. For this, we use a set of meta-materials of distinctive spectral responses, and THz waveforms are adaptively designed to match their spectral responses to the materials, respectively. With the prepared THz waveforms then we carry out a proof-of-principle experiment of THz substance imaging of a two-dimensional target constructed with those meta-materials.

#167967 - $15.00 USD Received 4 May 2012; revised 31 Jul 2012; accepted 20 Aug 2012; published 24 Aug 2012

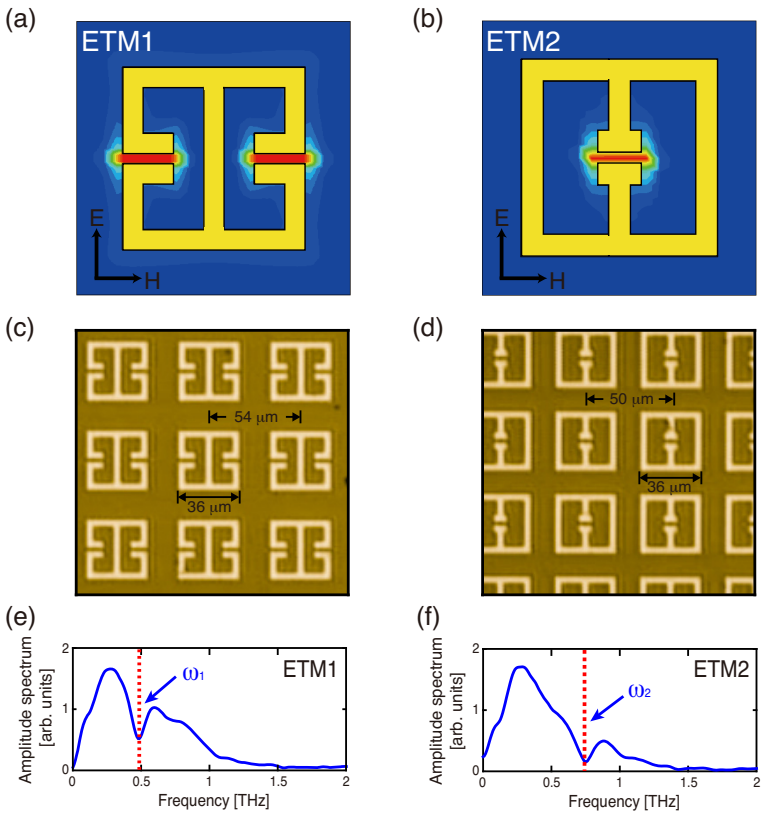

Fig. 1. Meta-material samples ETM1 and ETM2. (a, b) Electric field norms plotted at their resonance frequencies. (c, d) Microscope images of the fabricated samples. (e, f) Measured transmitted amplitude spectra of unshaped THz pulses. (Dotted lines indicate the calculated resonance frequencies.)

2. Sample preparation

For the test of the material classification based on THz pulse-shaping, we used meta-material samples of noticeable spectral feature in THz frequency range. We chose electrically resonant meta-materials (ETMs), in which magnetic response is suppressed by symmetry and thus purely electrically resonant response can be constructed [21]. In Figs. 1(a) and 1(b), the design of the two ETMs (ETM1 and ETM2) are shown. The norm of the electric field at resonance frequency is displaced, where the red regions in the gaps indicate strong local field enhancement. As the capacitance C of ETM1 is about two-times larger than that of ETM2, while their inductance L's are about the same, the resonance frequency, which is given by $\omega_o = 1/\sqrt{LC}$ for an RLC circuit, of ETM1 is red-shifted compared to that of ETM2.

The fabrication of the designed ETMs was carried out by using a conventional photolithographic method. Gold stripes of 150-nm thickness were arranged in a planar array geometry on a 500-μm-thick silicon substrate with a 15-nm-thick titanium adhesion layer. The fabricated ETMs are shown in Figs. 1(c) and 1(d). The density of each ETM was chosen so that the same amount of the power for an unshaped THz pulse transmitted through the samples. The lattice constants of ETM1 and ETM2 were chosen 54 and 50 μm, respectively. In Figs. 1(e) and 1(f), the measurements of the transmitted amplitude spectra are shown, where the resonance

#167967 - $15.00 USD Received 4 May 2012; revised 31 Jul 2012; accepted 20 Aug 2012; published 24 Aug 2012

frequencies of ETM1 and ETM2 are 0.47 and 0.77 THz, respectively.

3. Experimental procedure

Experimental demonstration was performed in a generic THz-TDS with a pulse-shaping add-on. The experimental setup is schematically shown in Fig. 2(a). Ultrafast optical pulses were produced from a Ti:sapphire mode-locked laser oscillator, and pulse-shaped by a spatial light modulator (SLM) placed in the Fourier plane of a 4-f geometry Martinez zero-dispersion stretcher [22]. The SLM consisted of 128 liquid crystal pixels of individual phase modulation for the wavelength range of 830-870 nm. For the spectral arrangement of the optical pulses, a pair of holographic grating of 1800 lines/mm groove density was used as well as a pair of cylindrical lens of focal length of 150 mm [12]. Then, the shaped optical pulses were focused on to a photoconductive antenna to generate shaped THz pulses. The generated THz radiation pulses were detected via optical gating method with a 2-mm-thick $\langle 110 \rangle$ ZnTe crystal in the far-field region, where the temporal profile measurement of the THz pulses was carried out. For the THz transmitted power measurement, we used temporal integration of the square of the temporal electric field measurement. It is noted that a direct THz power detection using a low-temperature bolometer, as shown in Fig. 2(a), could replace the THz-TDS of our experiment.

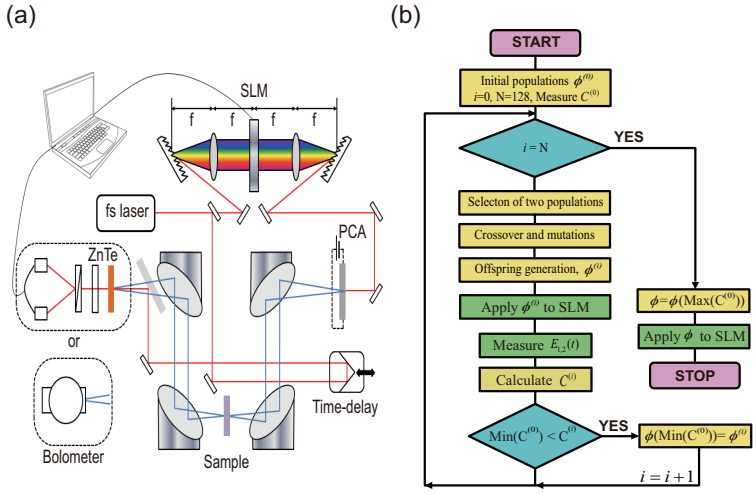

Fig. 2. (a) Schematic experimental diagram of THz pulse shaping with a spatial light modulator. (b) Adaptive feed-back loop implemented for the THz pulse profile optimization.

THz pulses were shaped with an adaptive feed-back algorithm, where the optimization target function was the spectral correlation difference C_1 defined as

$$C_1(\{E(\omega)\}) = \int \left(|t_1(\omega)E(\omega)|^2 - |t_2(\omega)E(\omega)|^2 \right) d\omega, \tag{1}$$

where $E(\omega)$ is the amplitude spectrum of the tested THz pulse and $t_{1,2}(\omega)$ are the amplitude transmission coefficients [23] of ETM1 and ETM2, respectively. So, a shaped THz waveform $E(\omega)$ which finds the biggest positive (negative) $C_1(\{E(\omega)\})$ can be used to detect the first (the second) among the two materials. Likewise, this method can be generalized for a larger set of material substances than two: Finding the i^{th} material among M different materials can be achieved by finding the biggest value for the correlation function, for example, $C_i(\{E(\omega)\})$

#167967 - $15.00 USD Received 4 May 2012; revised 31 Jul 2012; accepted 20 Aug 2012; published 24 Aug 2012

which can be defined as

$$C_i(\{E(\omega)\}) = 2\int |t_i(\omega)E(\omega)|^2 d\omega - \sum_{j=1}^{M}\int |t_j(\omega)E(\omega)|^2 d\omega, \quad (2)$$

where $t_i(\omega)$ is the amplitude transmission coefficient [23] of the i^{th} material.

As the spectral correlation function $C_1(\{E(\omega)\})$ is given linear to each spectral intensity $|E(\omega)|^2$, designing an optimal THz pulse shape $\{E(\omega)\}$ is mathematically straightforward. For example, the biggest $C_1(\{E(\omega)\})$ in Eq. (1) can be obtained by maximizing the spectral intensity $|E(\omega)|^2$ for those spectral components that satisfy $|t_1(\omega)| > |t_2(\omega)|$ and, at the same time, by minimizing $|E(\omega)|^2$ for $|t_1(\omega)| < |t_2(\omega)|$. However, as the pulse shaping procedure of THz waveforms is indirectly processed via temporal pulse shaping of optical pulses in the phase-only shaper, there exist practical limitations to the capability of precise THz pulse shaping. Therefore, we chose alternatively an adaptive search procedure for the design of optimal THz pulse shapes by sequentially increasing or decreasing $C_1(\{E(\omega)\})$, which intuitively verified two substances.

Figure 2(b) shows the optimization procedure of the adaptive THz pulse shaping with a feedback loop which was operated based on genetic search algorithm [24]. For the optimization passage, we used the single parameter $C_1(\{E^{(i)}(\omega)\})$ which was defined by the power difference of two THz signals through the two substances, ETM1 and ETM2, respectively. We first started with a set of 30 random phase vectors (populations). The series of initial 30 phase vectors was randomly generated within $[-\pi, \pi]$ and both the transmitted THz temporal profiles were measured by alternating the samples ETM1 and ETM2. The correlation function $C_1(\{E^{(i)}(\omega)\})$ was then evaluated for each phase vector. Once the measurements for all the initial phase vectors were completed, the phase vector that gave the smallest absolute value for C_1 was discarded, and a pair of phase vectors was selected among the others, and an off-spring phase vector was generated based on the crossover and roulette rules in the genetic algorithm, with the random phase change (mutations) of 3% of SLM pixel elements [24]. The newly constructed 30 phase vectors were then used for the next generation, and the procedure repeated itself for $N = 128$ iterations until the optimal phase vector was determined.

4. Results and discussion

Figure 3 shows the experimental adaptive search results for the biggest positive and negative correlation function C_1, respectively. In the first experiment, finding the biggest positive C_1 in Figs. 3(a-c), the optimization procedure found the THz programmed waveform that transmitted through ETM1 better than ETM2. The iterative measurements of C_1 during its positive maximization process are shown in Fig. 3(a). All of the correlation difference from the initial 30 phase vectors increased gradually during the feed-back loop evolution. During the total $N = 128$ iterations, adaptively found THz waveforms and their spectra changed significantly. The best value of correlation differences provided by the set of the 30 phase vectors increased from 4.2 to 10.3 (arb. unit) and the average increased from 2.0 to 8.5. With the best phase vector that gave the maximal correlation difference at the end of the 128 iterations, the measured THz waveforms transmitted through the samples ETM1 and ETM2 are, respectively, shown in Fig. 3(b). Their amplitude spectra plotted in Fig. 3(c) clearly show interesting frequency characteristics: Their spectral response difference is broadly located around 0.8 THz, near the resonance frequency 0.77 THz of ETM2, and relatively low spectral density around 0.5 THz, near the ETM1 resonance. This result is in an excellent agreement with the prediction provided in Sec. 3: Positive maximization of C_1 was achieved by increasing the spectral intensity $|E(\omega)|^2$ for the ω region that satisfied $|t_1(\omega)| > |t_2(\omega)|$, which was around 0.77 THz, and, at the same time, decreasing the spectral region for $|t_1(\omega)| < |t_2(\omega)|$, which was near 0.5 THz.

#167967 - $15.00 USD Received 4 May 2012; revised 31 Jul 2012; accepted 20 Aug 2012; published 24 Aug 2012

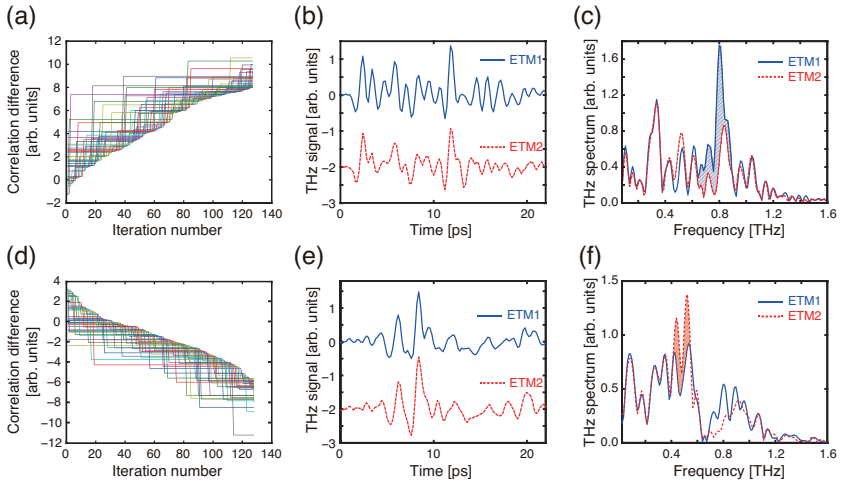

Fig. 3. (a,d) Measured correlation difference C_1 vs. the iteration number for the recognition of ETM1 and ETM2 substances, respectively. Measurement of the final THz waveforms (b,e) and their THz spectra (c,f).

So, the as-found THz waveform provided relatively high transmission through ETM1 compared to ETM2, and, therefore, the C_1 maximization was achieved. Likewise, the second experiment, finding the biggest negative C_1, is shown in Figs. 3(d-f), where the spectral density of the shaped THz pulse is mainly located around 0.5 THz, having significant spectral difference between the ETM1 and ETM2 transmission, as shown in Fig. 3(f). Although their spectral behaviors around 0.77 THz were not perfect, the as-found THz waveform minimized the spectral correlation C_1, as predicted.

Finally, we performed the substance imaging experiment with the adaptively achieved THz waveforms. The imaging target shown in Fig. 4(a) consisted of the two different THz metamaterials, where the left half square was filled with ETM1 and the right half with ETM2. Figure 4(b) shows the THz power imaging result with an unshaped THz pulse, which has little image contrast between the two ETM regions. On the other hand, the results shown in Figs. 4(c) and 4(d) were obtained by utilizing the adaptively found THz waveforms in Figs. 3(b) and 3(e), respectively, and the highly contrasting THz power images in Fig. 4(c) for the biggest positive C_1 and Fig. 4(d) for the biggest negative C_1, respectively, are clearly demonstrated. Therefore, the two ETM regions unresolved by the initial unshaped THz pulse are clearly distinguished as a result of evolutionary THz pulse shaping. Figs. 4(e) and 4(f) show the measured THz power along the lateral X-positions marked with dashed lines in Figs. 4(c) and 4(d), which results indicate that the relative contrast, defined by $P_{\text{contrast}} = (P_1 - P_2) \,/\, (P_1 + P_2)$, where P_1 and P_2 are the transmitted THz powers in the ETM1 and ETM2 regions, respectively, is enhanced by a factor of 9.5 compared to the initial power fluctuation level. Therefore, the shaped THz pulse shaping system demonstrates enhanced THz substance contrast imaging as a result of selective attenuation sensitivity of the shaped THz pulses coupled with the material responses.

5. Conclusions

In summary, this work has demonstrated that THz material substance imaging is achieved through a THz pulse-shaping method. THz pulse shaping has provided frequency-modulated THz pulses and material specific absorption change. During the procedure of evolutionary algorithm, the increase or decrease of spectral correlation difference has made it possible to

#167967 - $15.00 USD Received 4 May 2012; revised 31 Jul 2012; accepted 20 Aug 2012; published 24 Aug 2012

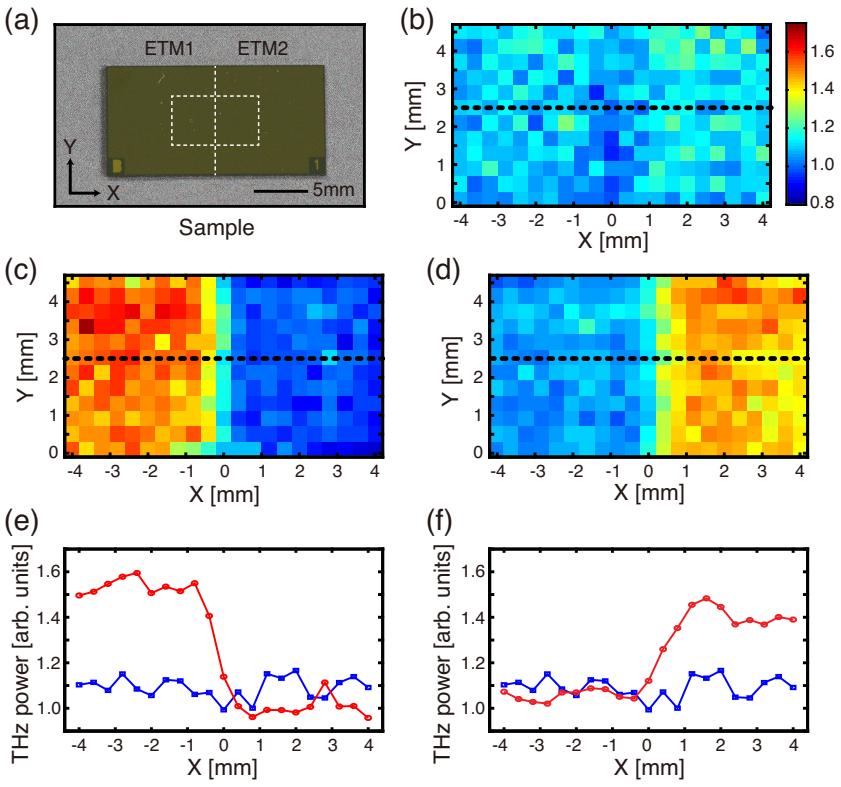

Fig. 4. (a) An imaging target consists of two different THz meta-material regions, where the left half square is filled with ETM1 of 0.5 THz resonance frequency and the right half with the other with 0.8 THz. (b-d) Measured THz power images with three different THz pulses: (b) the near zero, (c) the biggest positive, and (d) the biggest negative correlation-difference phase-mask arrays, respectively. (e,f) Measured THz power (red) along the lateral X-positions marked with dashed lines in (c,d), respectively, where the reference measurement (blue) is from (b).

distinguish between the given materials. In the imaging experiments, the shaped THz pulse imaging system has successfully identified the localized substance distribution. The observed image contrast enhancement of 9.5 times is achieved compared to the initial power fluctuation level of unshaped THz pulses. It is hoped that this method could be extended to frequency-dependent functional biological and medical imaging, and nondestructive inspection in THz frequency region.

Acknowledgments

This work was supported in part by Basic Science Research Programs [2009-0090843, 2010-0013899, 2009-0083512] and in part by the World Class Institute Program [WCI 2011-001] through the National Research Foundation of Korea funded by the Ministry of Education, Science and Technology of Korea.

#167967 - $15.00 USD Received 4 May 2012; revised 31 Jul 2012; accepted 20 Aug 2012; published 24 Aug 2012